Increased Photovoltaic Power Output via Diffractive Spectrum Separation

Ganghun Kim, Jose A. Dominguez-Caballero, Howard Lee, Daniel J. Friedman, and Rajesh Menon

Increased photovoltaic power output via diffractive spectrum separation

Ganghun Kim[1], Jose A. Dominguez-Caballero[2], Howard Lee[3], Daniel Friedman[4] and Rajesh Menon[1]

[1]*Department of Electrical and Computer Engineering, University of Utah, Salt Lake City, UT 84112, USA.* [2]*Department of Mechanical Engineering, Massachusetts Institute of Technology, Cambridge, MA 02139, USA.* [3]*Stion Inc, San Jose, CA 95119 USA.* [4]*National Renewable Energy Laboratory, Golden, CO 80401, USA.*

In this Letter, we report the preliminary demonstration of a new paradigm for photovoltaic-power generation that utilizes a broadband diffractive-optical element (BDOE) to efficiently separate sunlight into laterally-spaced spectral bands. These bands are then absorbed by single-junction photovoltaic cells, whose bandgaps correspond to the incident spectral bands. We designed such BDOEs by utilizing a modified version of the direct-binary-search algorithm. Grayscale lithography was used to fabricate these multi-level optics. They were experimentally characterized with an overall optical efficiency of 70% over a wavelength range of 350nm-1100nm, which was in excellent agreement with simulation predictions. Finally, two prototype devices were assembled; one with a pair of Copper Indium Galium Selenide (CIGS)-based photovoltaic devices, and another with GaAs and c-Si photovoltaic devices. These devices demonstrated an increase in output peak electrical power of ~42% and ~22%, respectively under white-light illumination. Due to the optical-versatility and manufacturability of the proposed BDOEs, the reported spectrum-splitting approach provides a new approach towards low-cost solar power.

Single p-n junction photovoltaic devices are fundamentally limited in the efficiency with which they can convert sunlight primarily because photons of energy lower than the bandgap are not absorbed, and photons of energy much higher than the bandgap lose their excess energy as heat via a process referred to as thermalization (1). The theoretical maximum efficiency for a single-junction photovoltaic device under unconcentrated sunlight is ~33% (2). On the other hand, multi-junction photovoltaic devices are capable of efficiencies greater than 40% (3, 4). Typically, such devices are vertically stacked

junctions, with the bandgap of each junction decreasing from top to bottom. The highest energy photons are absorbed at the top junction. Subsequent junctions absorb lower energy photons. Such devices can be epitaxially grown (4) or mechanically stacked (5). Mechanically stacked devices suffer from significant optical losses due to reflections at the interfaces. Epitaxially grown devices suffer from the challenge of fabricating junctions with the combinations of bandgaps that are optimal for the solar spectrum. The current produced by each junction must be the same, since the epitaxially grown junctions are typically connected in series. Furthermore, epitaxial devices require a tunnel junction at the interface between each p-n junction in the structure, which increases the complexity of the fabrication process. In this Letter, we describe the use of a thin broadband diffractive-optical element (BDOE) designed to efficiently separate and concentrate incident illumination (eg. Sunlight) into pre-determined bands that illuminate laterally separated photovoltaic devices of matching bandgaps. This approach avoids the afore-mentioned disadvantages of conventional multi-junction devices while utilizing the broad solar spectrum efficiently.

Spectral separation of sunlight may be achieved via refraction, interference or diffraction (6). Prisms enable spectral separation via dispersive refraction. However, they are impractical for scaling to large areas due to the volume and weight requirements. Furthermore, they offer very little control over the spatial position of the bands as well as the choices of band edges. Interference, primarily via dichroic and multi-layer mirrors, has been used to demonstrate spectral splitting for photovoltaics (7,8). However, the geometry of such devices precludes scaling to large areas and limits the number of bands that can be separated. Conventional gratings enable spectral separation via diffraction;

however, they typically suffer from low diffraction efficiency as well as poor control of the spatial position of the spectral bands.

In contrast, we utilize a non-conventional approach for the design of a multi-level BDOE that spatially separates and concentrates distinct spectral bands as illustrated in Fig. 1(A). We call this BDOE a polychromat. A conventional binary-search algorithm was adapted for the design (9). This nonlinear optimization algorithm was reformulated to solve a multi-dimensional constrained problem with an objective function designed to maximize the polychromat's average optical efficiency. The polychromat's optical efficiency at a specific wavelength is defined as the ratio of the radiant energy at that wavelength incident on its optimal absorber divided by the total radiant energy at that wavelength incident on the polychromat. The set of feasible solutions found by the algorithm was constrained to those that matched the required fabrication constraints.

A one-dimensional polychromat that separates sunlight (350nm-1300nm) into two bands: 350nm-800nm and 801nm-1100nm, is shown in Fig. 1(B). The polychromat is comprised of 1000 discrete pixels, each of size 10μm. On the reconstruction plane, each spectral band covers approximately half the area of the polychromat, corresponding to a concentration factor of ~2X. The distance between the polychromat and the reconstruction plane is dictated primarily by diffraction angles and hence, the pixel size. In the current design, the distance was set at 14cm but it can be reduced to less than 3cm by choosing a pixel size of 1μm or smaller (11). The design was constrained to 8 height levels as shown in Fig. 1(B). A magnified view of a selected region is shown in Fig. 1(C), where the discrete 10μm-wide pixels as well as 8 discrete height levels are apparent.

The polychromat was fabricated using grayscale-optical lithography (10). An optical micrograph is shown in Fig. 2(A). Figure 2(B) shows a magnified view of an optical profilometer image of a small portion of the same polychromat. The pixels of width 10µm as well as the multi-level structure are evident. The entire device was comprised of three repeating units in order to account for the assumed periodic boundary conditions, covering an area of about 3cm X 3cm (11).

The polychromat performance was characterized by measuring the spectrum as a function of position in the reconstruction plane, a spatial-spectral map. Each row in the map corresponds to the spatial distribution of the diffracted light power at the respective wavelength. The measured map is compared against the simulated map in Figs. 2(C) and (D). In addition, the measured optical efficiency is compared to the simulated efficiency in Figs. 2(E) and (F). The optical efficiency at a given wavelength in the solid blue curve refers to the efficiency with which the photons are allocated to the sub-cell on the left. The green dashed curve refers to the sub-cell on the right. The spectrally-averaged optical efficiency is 70%. Note that the map and efficiency spectra agree well with the simulations. It must be pointed out that this is the first experimental demonstration of high efficiency ultra-broadband imaging with diffractive optics. Much higher optical efficiencies are expected with more height levels (11).

We performed electrical characterization with both a pair of CIGS cells as well as Si/GaAs cells. The two CIGS cells were designed with bandgaps of 1.05eV and 1.5eV. Each cell was placed on a substrate mounted on a single-axis scanning stage with its axis orthogonal to the plane of the polychromat, and electrical characteristics measured independently. The distance between the polychromat and the plane containing the cells

was set with an optical track to within +/-1mm. The cells were aligned to the spectra visually (11). Note that in order to achieve sufficient spatial coherence, the light output from the source had to be expanded over a long distance (1.5m), which resulted in the incident intensity at the polychromat plane being ~4 orders of magnitude smaller than that of the standard AM1.5 spectrum (11). Under these conditions, the open-circuit voltage is expected to be ~0.25-0.5V lower than that observed under 1sun, which is consistent with the measured results shown in Figs. 3 and 4 for CIGS and Si/GaAs cells, respectively. Furthermore, at low illumination intensities, even a small shunt resistance decreases the fill factor significantly (as can be seen for the CIGS cells). The reference measurements are shown as thin red lines, while those with the polychromat are shown as thick blue lines. The polychromat redirects higher-energy photons that would otherwise fall onto the low-bandgap cell (CIGS or Si) to the high-bandgap cell (CIGS or GaAs), and likewise lower-energy photons from the high-bandgap (where they wouldn't be absorbed) to the low-bandgap cell. In other words, the polychromat concentrates input light of each spectral band by a factor of ~2 (the ratio of the area of the polychromat to the area of each cell). For the high-bandgap cell, this results in an increase in short-circuit current density, J_{sc} (Figs. 3A and 4A). The increased flux also tends to increase the open-circuit voltage, V_{oc}. Those higher-energy photons that are redirected to the high-bandgap cell are converted to current at a higher voltage than would be the case in the absence of the polychromat, *i.e.*, the low-bandgap cell would have absorbed those photons. As a result, the efficiency of the high-bandgap cell increases with the utilization of the polychromat. On the other hand, the low-bandgap cell loses the higher-energy photons but gains lower-energy photons. Unfortunately, since the halogen lamp used in our

5

experiments had significantly fewer infrared photons compared to visible photons, the

total power density of the gained low-energy photons was not sufficient to compensate

for the loss of the high-energy photons (11). As a result, the J_{sc} and V_{oc} both drop slightly

for the low-bandgap cell (Figs. 3B and 4B). Therefore, a small drop in efficiency of the

low-bandgap cell is observed (Figs. 3D and 4D). However, this decrease is more than

compensated by the increased output power from the high-bandgap cell. Thereby, the

total output power density (added from both cells) with the polychromat is increased by

~42% for CIGS (Fig. 3C) and ~22% for Si/GaAs (Fig. 4C).

Numerical simulations indicate that ideal spectrum splitting with these pairs of

cells can result in an increase in output power-density of ~68% (11). Much of the

discrepancy with the measured results can be accounted by the decrease in the

polychromat efficiency close to the band-edge and the low illumination level. The results

as well as other simulations that assume AM1.5 (11) incident spectrum suggest that an

integrated design approach for the polychromat that takes into account the cell

performance under specific illumination conditions could achieve power-density

increases that are closer to the theoretical limits. Nevertheless, our initial results clearly

indicate the potential of using a polychromat for efficient spectrum-splitting.

BDOEs may be designed to separate more than 2 bands, allowing for even higher

conversion efficiencies. Another interesting advantage of this approach is that by

avoiding the thermalization losses in the low bandgap sub-cell, we could reduce its

temperature. In our preliminary experiments, the polychromat covered only a small area

(3cm X 3cm). For a practical photovoltaic system, the area must be scaled to ~1m X 1m.

This is possible in a cost-effective manner with manufacturing methods such as roll-to-

roll processing (12). Although III-V materials such as GaAs are currently too expensive to use under low or no concentration, recent advances in thin-film GaAs manufacturing (13) are rapidly decreasing costs and the proposed spectrum-splitting approaches can play a major role in achieving high-photovoltaic-system efficiencies with only marginal increase in costs.

References:

1. Henry, C. H. Limiting efficiencies of ideal single and multiple energy gap terrestrial solar cells. *J. Appl. Phys.* **51**(8), 4494-4500 (1980).

2. Miller, O. D., Yablonovitch, E. & Kurtz, S. R. Intense internal and external fluorescence as solar cells approach the Shockley-Queisser efficiency limit. *arXiv:1106.1603v3.* (2011).

3. Geisz, J. F., Friedman, D. J., Ward, J. S., Duda, A., Olavarria, W. J., Moriatry, T. E., Kiehl, J. T., Romero, M. J., Norman, A. G. & Jones, K. M. 40.8% efficient inverted triple-junction solar cell with two independently metamorphic junctions. *Appl. Phys. Lett.* **93**(12): 123501 (2008).

4. King, R. R., Law, D. C., Edmondson, K. M., Fetzer, C. M., Kinsey, G. S., Yoon, H., Sherif, R. A. & Karam, N. H. 40% efficient metamorphic GaInP/GaInAs/Ge multijunction solar cells. *Appl. Phys. Lett.* **90** 183511 (2007).

5. Fraas, L. M., Avery, J. E., Martin, J., Sundaram, V. S., Girard, G., Dinh, V. T., Davenport, T. M., Yerkes, J. W. & O'Neil, V. S. Over 35-percent efficient GaAs/GaSb tandem solar cells. *IEEE Trans. Electr. Dev.* **37**(2): 443–449 (1990).

6. Imenes, A. G. & Mills, D. R. Spectral beam splitting technology for increased

conversion efficiency in solar concentrating systems: a review. *Solar Energy Materials and Solar Cells* **84**(1-4) 19–69 (2004).

7. Mitchell, B., Peharz, G., Siefer, G., Peters, M., Gandy, T., Goldschmidt, J. G., Benick, J., Glunz, S. W., Bett, A. W. & Dimroth, F., Four-junction spectral beam-splitting photovoltaic receiver with high efficiency. *Prog. Photovolt: Res. Appl.* **19**(1) 61-72 (2011).

8. Barnett, A.*, et al*. Very high efficiency solar cell modules. *Prog. Photovolt: Res. Appl.* **17**(1) 75–83 (2009).

9. Kim, G., Dominguez-Caballero, J-A. &R. Menon. Design and analysis of multi-wavelength diffractive optics. *Opt. Exp.* **20**(2), 2814-2823 (2012).

10. Levy, U. *et al.* Design, fabrication, and characterization of circular Dammann gratings based on grayscale lithography. *Opt. Lett.* **35**(6), 880- 882 (2010).

11. Details can be found in supplementary information.

12. Ahn, S. H. and Guo, L. J., High-speed roll-to-roll nanoimprint lithography on flexible plastic substrates. *Adv.   Mater.* **20**(11)**,** 2044–2049 (2008).

13. See cells from Alta Devices listed in Green, M. A. Emery, K. Hishikawa, Y. Warta W. and Dunlop E. D. Solar cell efficiency tables (version 38). *Prog. Photovolt: Res. Appl.* **19** 565 (2011).

Supplementary Information accompanies the paper online.

Competing Interests statement. None.

Methods.

The spectrum at each point in the reconstruction plane is measured with a spectrometer that has a 50µm aperture fiber input. The fiber is mounted on a single-axis stage that is then scanned across the reconstruction plane. Note that the polychromat and the reconstructed diffraction pattern are 1-D.

Author Contributions. G. K. designed the polychromat, and performed the optical and electrical characterization. J. A. D-C. designed the polychromat and the optical experiments, analyzed the results and edited the manuscript. H. L. provided the CIGS solar cells and edited the manuscript. D. F. provided the GaAs solar cells and edited the manuscript. R. M. designed and performed experiments, analysed results, performed simulations, and wrote the manuscript.

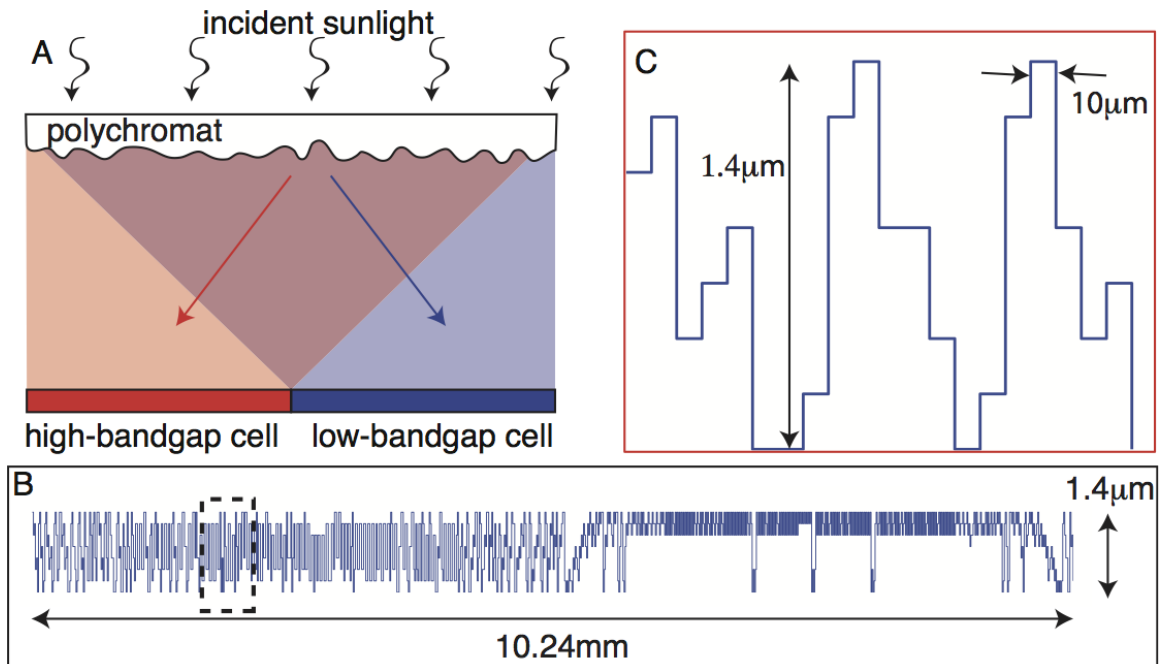Correspondence and requests for materials should be addressed to R. M. (rmenon@eng.utah.edu).

Fig 1: (A) A polychromat (a broadband diffractive-optical element or BDOE) separates incident sunlight into two bands, each of which illuminate neighbouring solar cells with matched bandgaps. (B) An example design of a polychromat represented by the height distribution of its pixels. See text for details. (C) Magnified view of several pixels of the dashed region of the polychromat in (B). Note the 8 height levels.
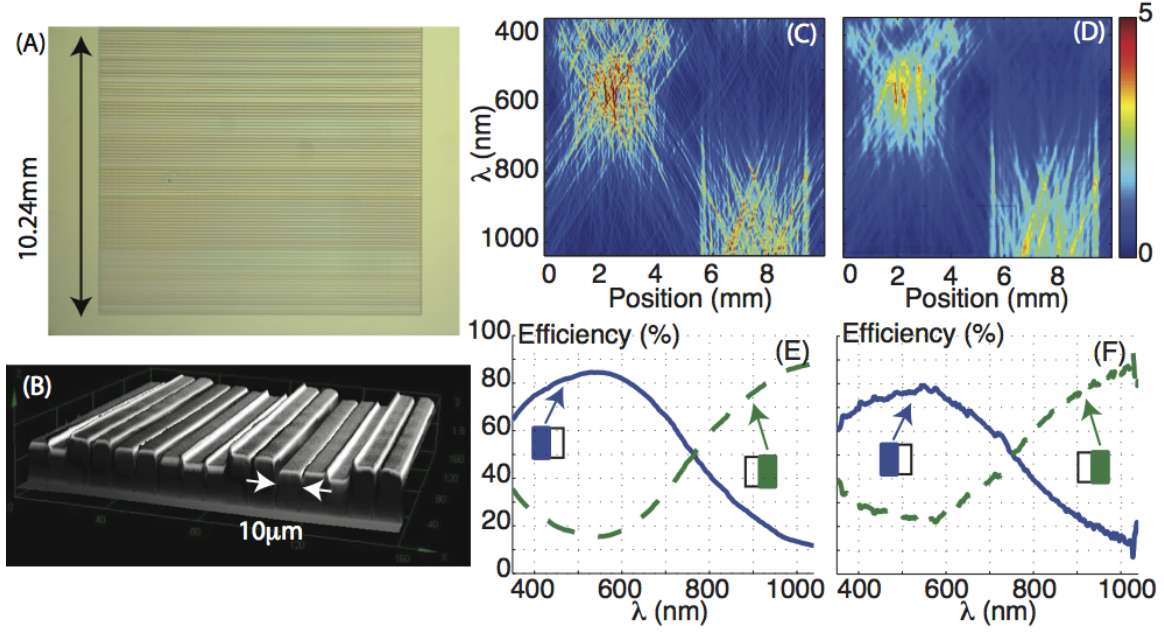
Fig. 2: (A) Bright-field image of a polychromat. (B) Magnified optical profilograph of a section of the polychromat. Spectral-spatial map at the polychromat reconstruction plane: (C) simulated and (D) measured. Optical efficiency of the polychromat as a function of wavelength: (E) simulated and (F) measured. The solid and dashed curves represent light diverted to the high- and low-bandgap cells, respectively.
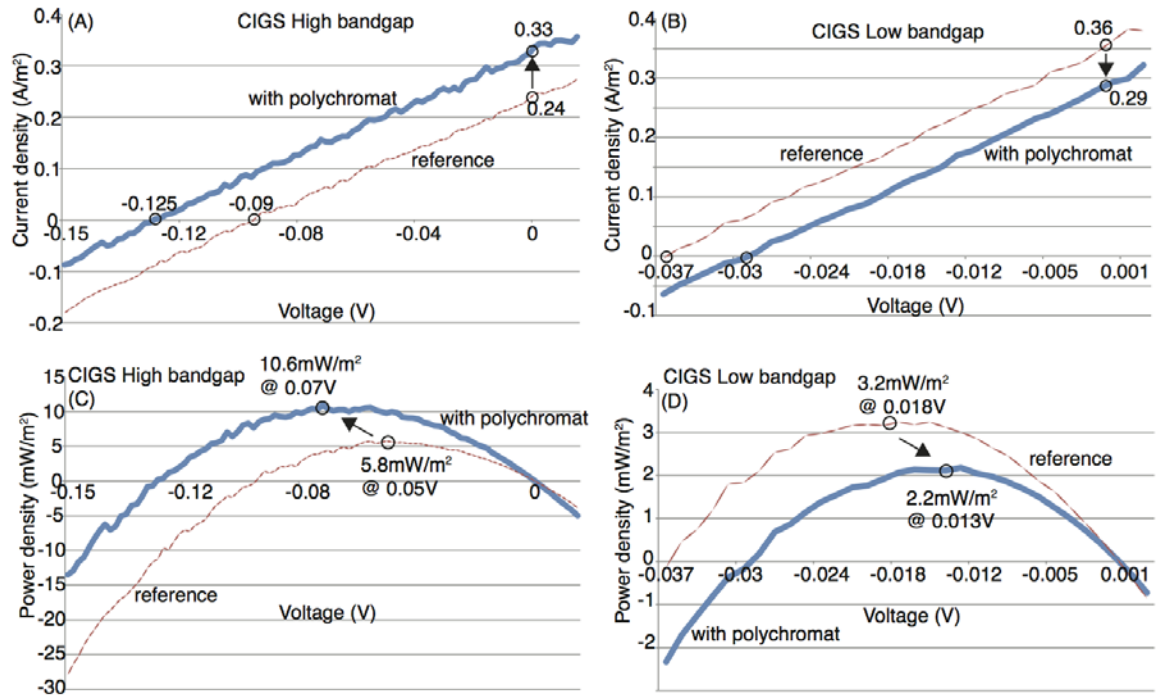
Fig. 3: Electrical characterization results of CIGS cells. Current-density as a function of bias voltage for the high-bandgap (A) and low-bandgap (B) CIGS cells. Power-density as a function of bias voltage for the high-bandgap (C) and low-bandgap (D) CIGS cells. The thin red and thick blue curves represent the measurements in the absence of and presence of the polychromat, respectively.
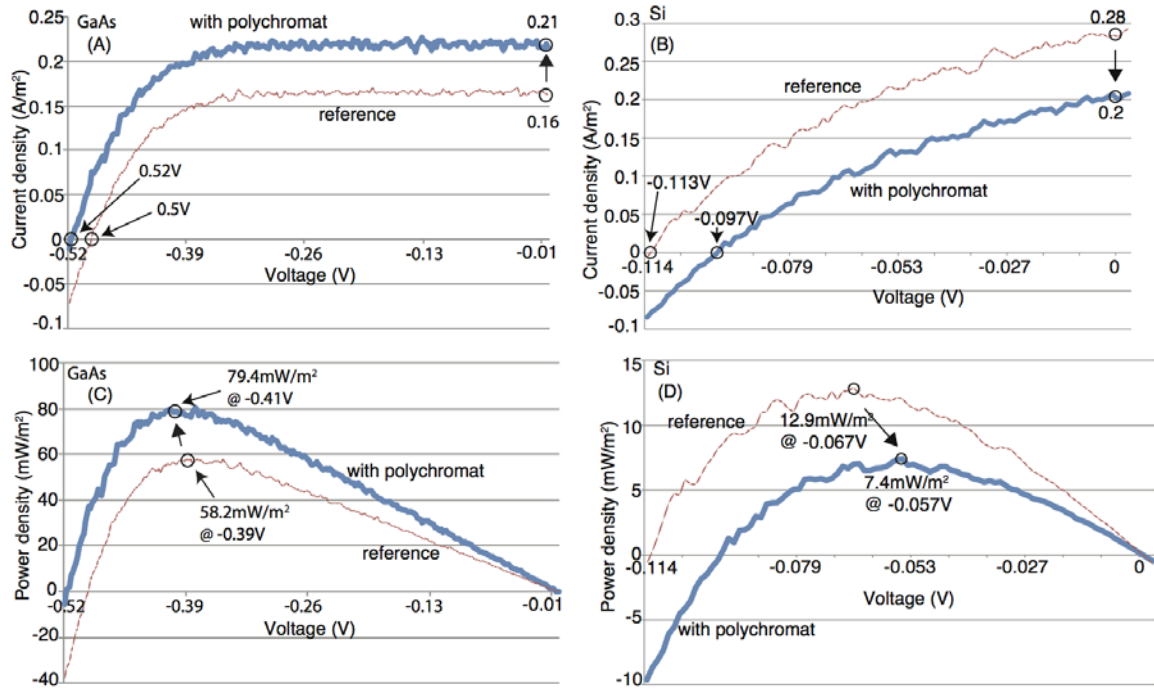
Fig. 4: Electrical characterization results of GaAs and Si cells. Current-density as a function of bias voltage for the GaAs (A) and Si (B) cells. Power-density as a function of bias voltage for the GaAs (C) and Si (D) cells. The thin red and thick blue curves curves represent the measurements in the absence of and presence of the polychromat, respectively.